Electronic Supplementary Material (ESI) for Physical Chemistry Chemical Physics.

Supporting Information

Property-Activity Relations of Multifunctional Reactive Ensembles in Cation-Exchanged Zeolites: A Case Study of Methane Activation on Zn^{2+}-Modified Zeolite BEA

Alexander A. Kolganov,[1] *Anton A. Gabrienko,*[1] *Ivan Yu. Chernyshov,*[2] *Alexander G. Stepanov,*[1] *Evgeny A. Pidko*[3,4*]

[1]Boreskov Institute of Catalysis, Siberian Branch of the Russian Academy of Sciences, Prospekt Akademika Lavrentieva 5, Novosibirsk 630090, Russia

[2]TheoMat group, ChemBio Cluster, ITMO University, Lomonosova 9, St. Petersburg, 191002, Russia

[3] Inorganic Systems Engineering group, Department of Chemical Engineering, Faculty of Applied Sciences, Delft University of Technology, Van der Maasweg 9, Delft 2629 HZ, The Netherlands

[4]TsyfroCatLab Group, University of Tyumen, Volodarskogo St.6, Tyumen 625003, Russia

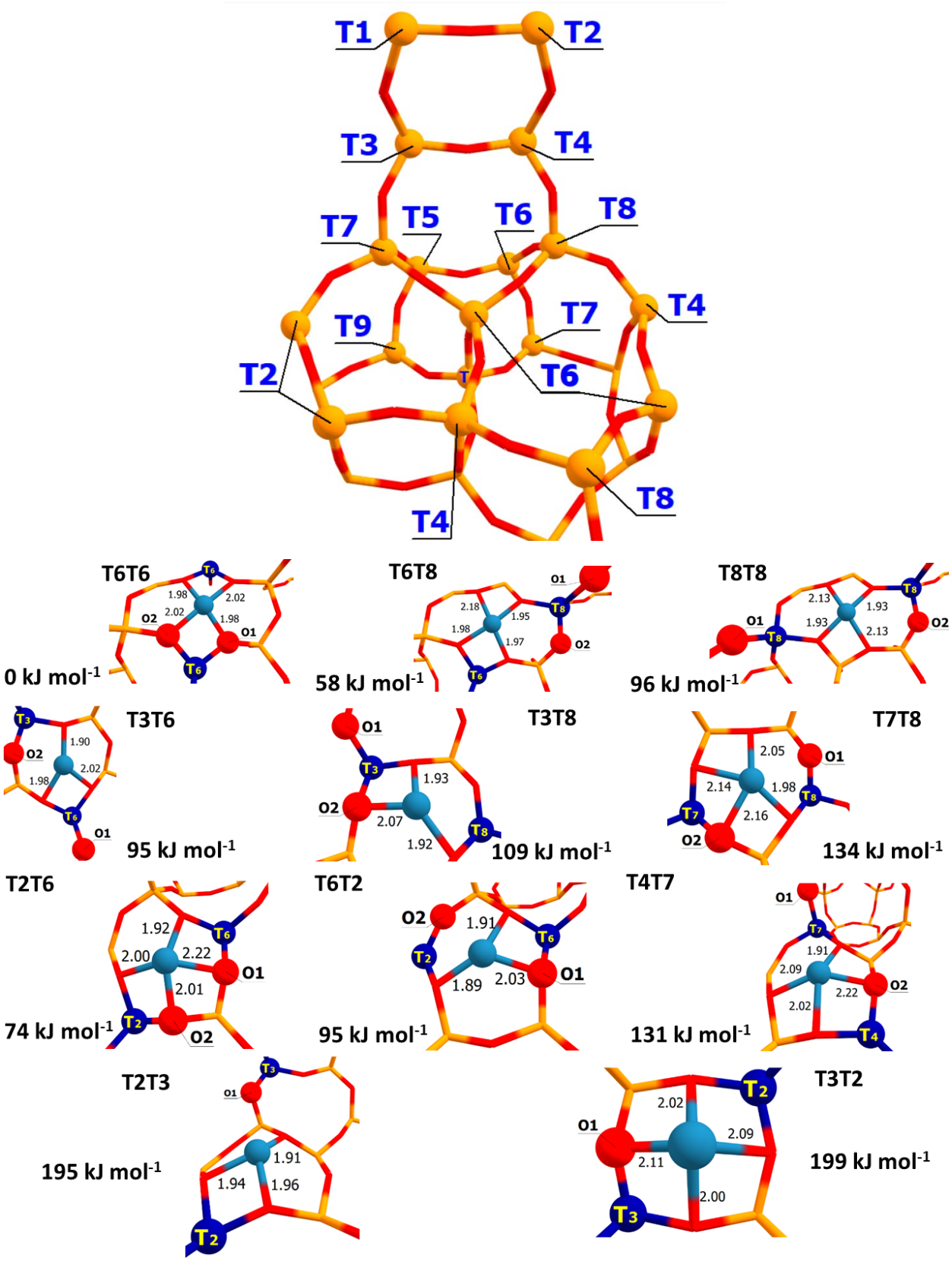

Figure S1. Different T sites in the BEA zeolite framework. Structure and relative stability of the Zn^{2+} cations placed in different locations within the BEA zeolite framework. All distances are shown in Å

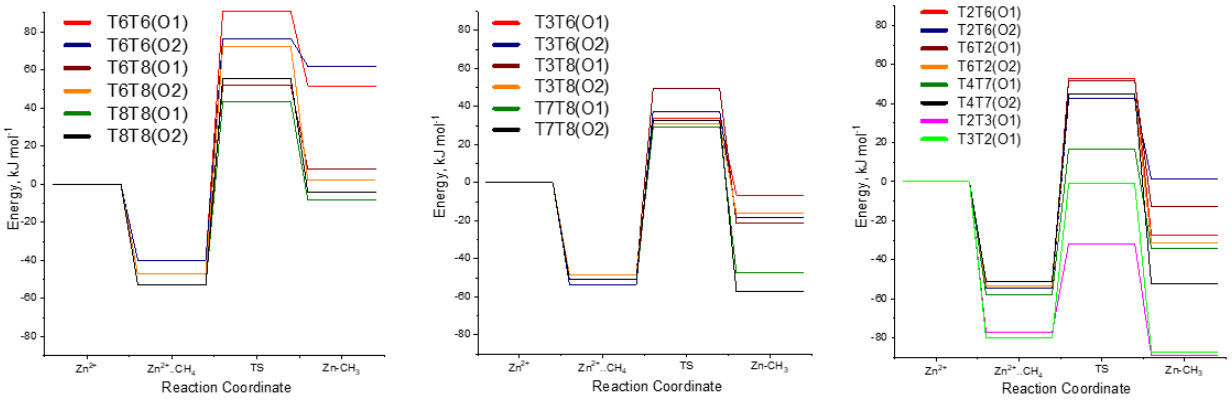

Figure S2. Energy diagrams for all considered methane activation reactions.

Table S1. Scaling coeffiecients for IR frequencies calculations

$CO(\nu_{C\equiv O})$	$CH_3CN(\nu_{C\equiv N})$	$C_5H_5N(\nu_{19})$	CH_4, (ν_1)	$C_4H_4NH(\nu_{N-H})$	CH_3CCH (ν_{C-H})
1.008	0.985	1.011	0.978	0.978	0.975

Table S2. Relative zeolite model stabilites, $\Delta E_{int}^{\neq}$,$\Delta E_{app}^{\neq}$,ΔE_r values and methane activation transition state imaginary frequencies for each considered $Zn_{EF}^{2+}\cdots O_F^{2-}$.

Configuration	Relative stability, kJ/mol	$\Delta E_{int}^{\neq}$, kJ/mol	$\Delta E_{app}^{\neq}$, kJ/mol	ΔE_r, kJ/mol	Imaginary frequencies, cm^{-1}/i
T6T6O1	0	131	91	52	907
T6T6O2		117	77	62	788
T6T8O1	58	99	52	8	1058
T6T8O2		120	72	2	920
T8T8O1	96	96	43	-8	1098
T8T8O2		109	56	-4	901
T3T6O1	95	88	34	-7	1017
T3T6O2		91	37	-19	986
T3T8O1	110	98	49	-26	1025
T3T8O2		79	31	-16	963
T7T8O1	134	80	29	-48	998
T7T8O2		84	33	-57	1021
T2T6O1	74	107	53	-27	961
T2T6O2		97	42	1	1029
T6T2O1	95	105	52	-13	992
T6T2O2		98	45	-31	1011
T4T7O1	131	74	17	-34	1052
T4T7O2		103	45	-52	1020
T2T3O1	195	46	-32	-89	1011
T3T2O1	199	79	-1	-87	1087

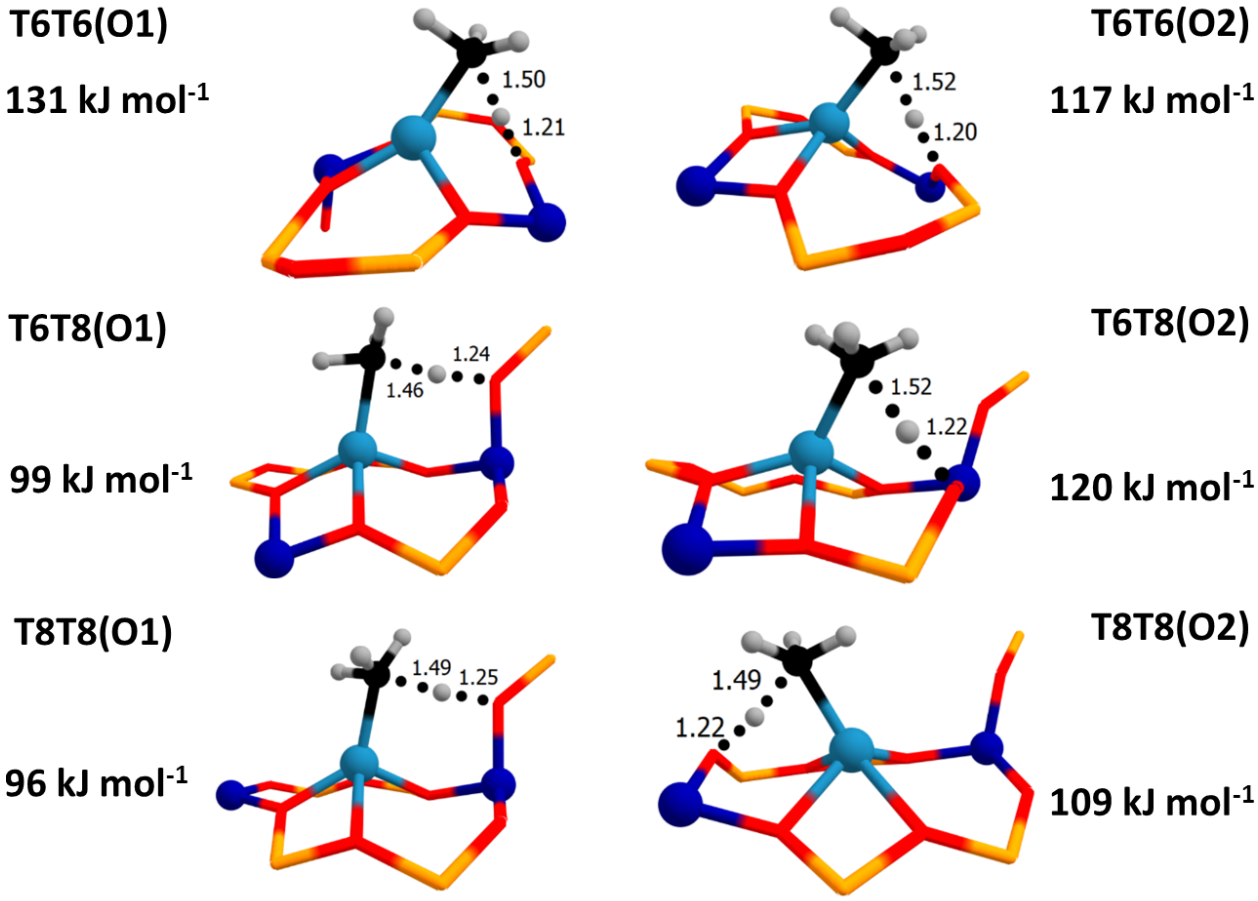

Figure S3. Geometries of the activation barriers of T6T6, T6T8 and T8T8 configuration.

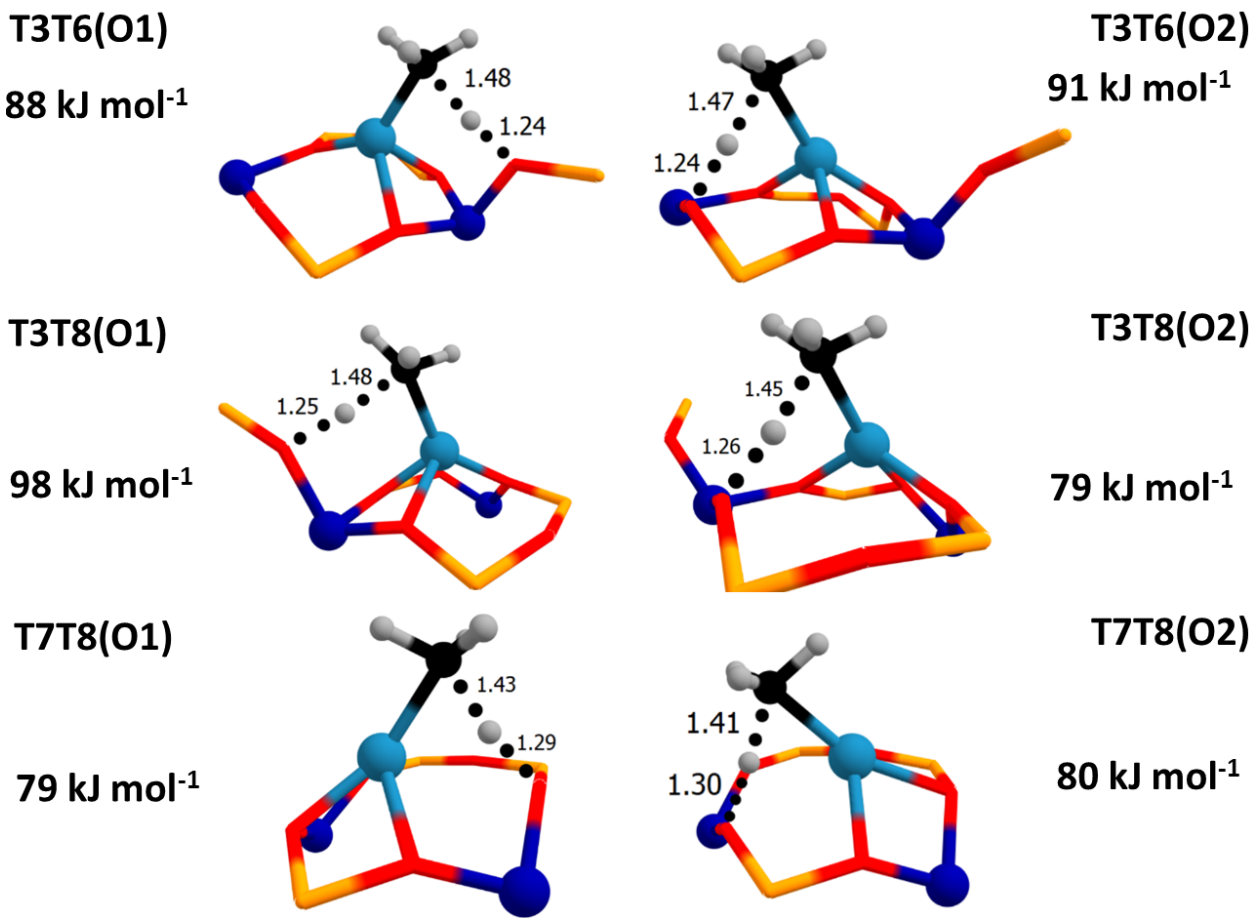

Figure S4. Geometries of the activation barriers of T3T6, T3T8 and T7T8 configurations.

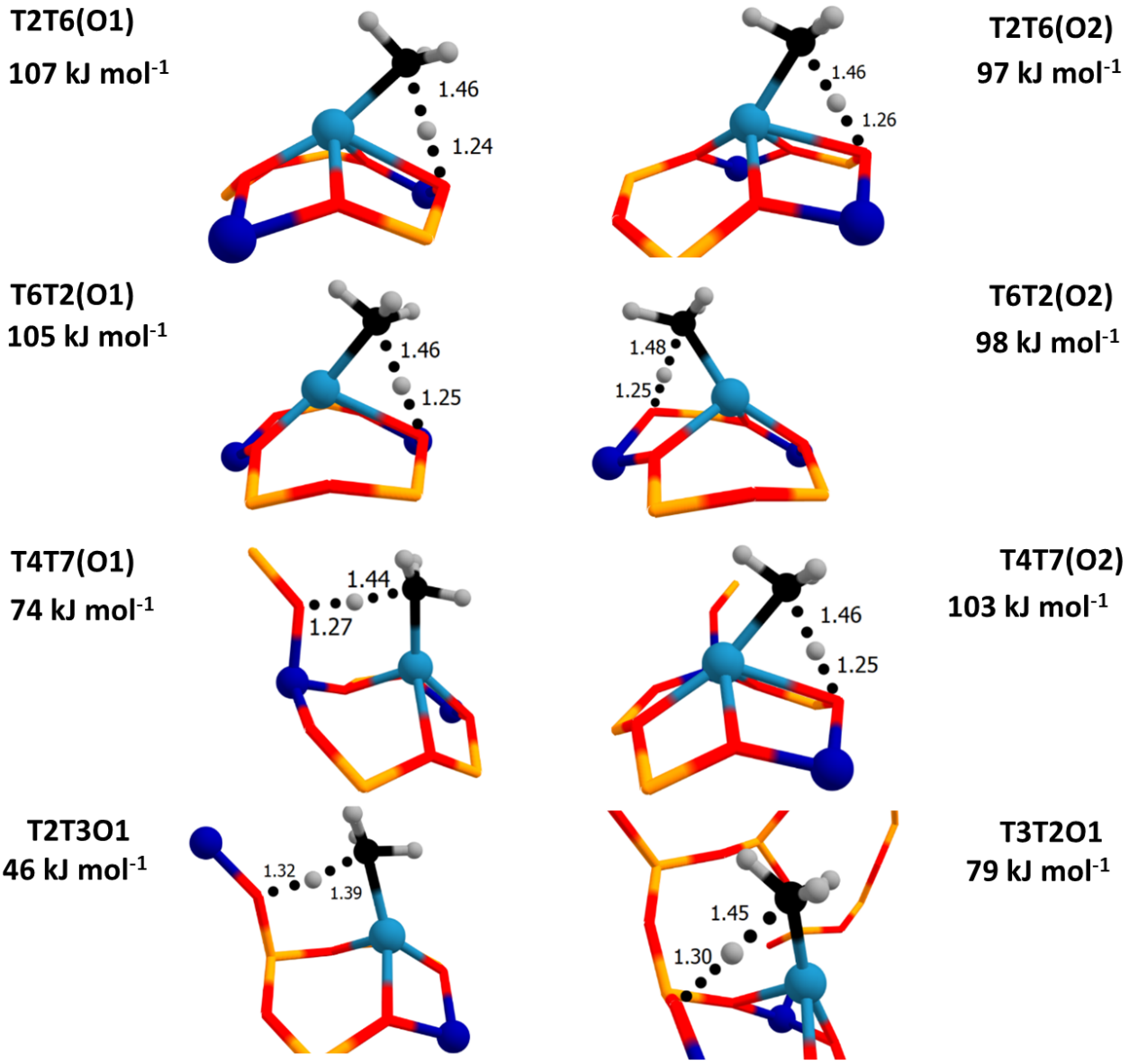

Figure S5. Geometries of the activation barriers of T2T6, T6T2, T4T7, T2T3 and T3T2 configurations.

Table S3. C–H and O_z–H distances in transition states and respective bond orders. The O_z denotes zeolite lattice oxygen atom.

Configuration	d(C–H), Å	d(O–H), Å	Bond order (C–H)	Bond order (O–H)
T6T6O1	1.501	1.210	0.332	0.499
T6T6O2	1.516	1.201	0.325	0.514
T6T8O1	1.461	1.243	0.393	0.481
T6T8O2	1.516	1.216	0.334	0.493
T8T8O1	1.494	1.249	0.371	0.487
T8T8O2	1.490	1.223	0.353	0.487
T3T6O1	1.478	1.240	0.365	0.482
T3T6O2	1.474	1.241	0.361	0.474
T3T8O1	1.476	1.252	0.368	0.466
T3T8O2	1.445	1.257	0.387	0.467
T7T8O1	1.426	1.287	0.399	0.436
T7T8O2	1.400	1.313	0.419	0.418
T2T6O1	1.457	1.238	0.366	0.472
T2T6O2	1.462	1.260	0.368	0.457
T6T2O1	1.457	1.250	0.371	0.469
T6T2O2	1.481	1.245	0.353	0.463
T4T7O1	1.440	1.267	0.407	0.465
T4T7O2	1.458	1.249	0.371	0.466
T2T3O1	1.448	1.296	0.447	0.419
T3T2O1	1.391	1.317	0.381	0.427

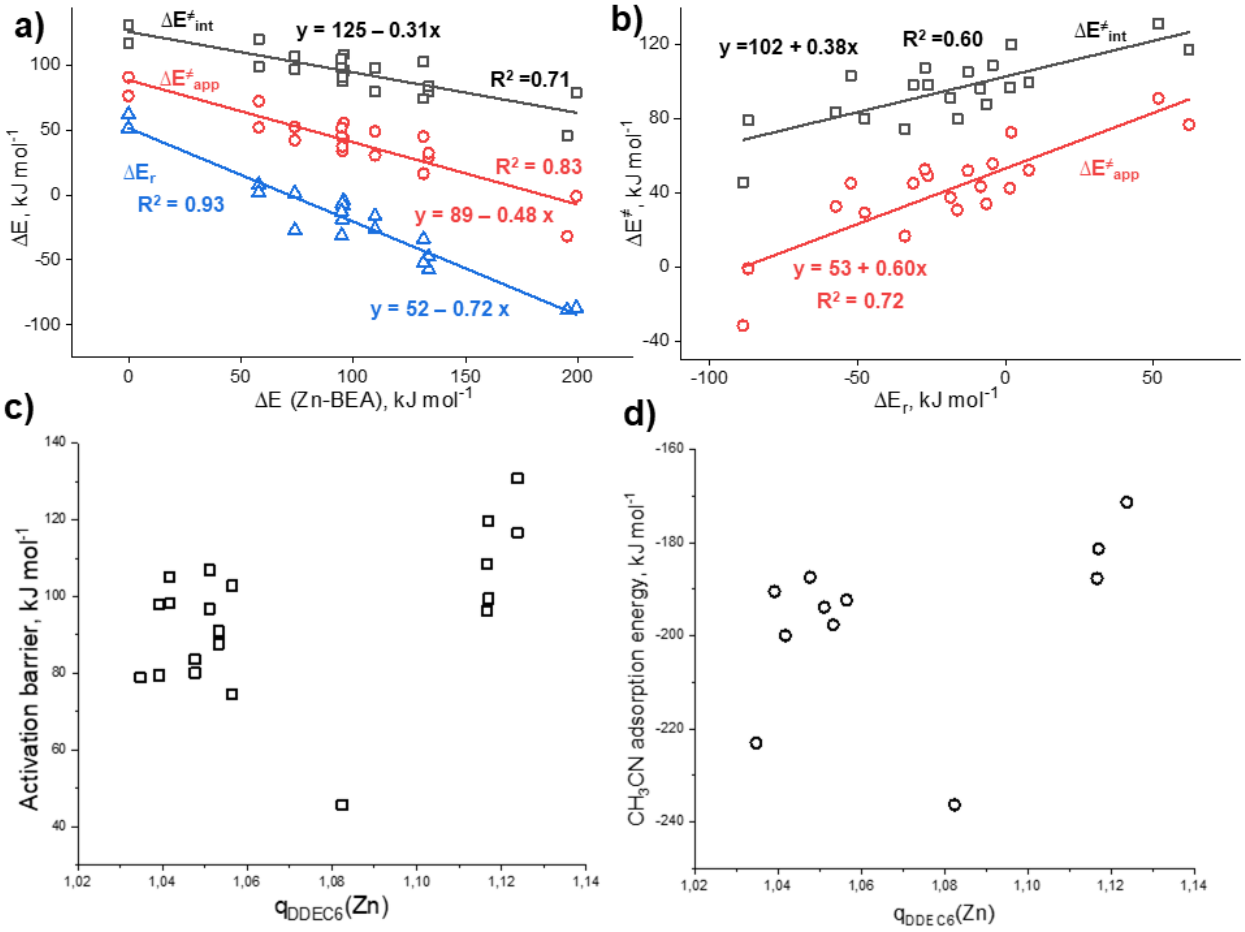

Figure S6. Correlations between the relative Zn-BEA stability and $\Delta E_{app}^{\neq}$, $\Delta E_{int}^{\neq}$, ΔE_r (a). The relationships between the reaction energy and the activation barriers (b). The relationships between the DDEC6 charges on Zn atoms and methane activaiton barriers (c). The relationships between the DDEC6 charges on Zn atoms and CH_3CN adsoprtion energies (d).

Table S4. Adsorption energies of the basic probes and CH_4; DDEC6 charges of Zn atoms.

	CO		CH_3CN		C_5H_5N		CH_4		q_{DDEC6}(Zn)
	$\Delta E_{ads,}$ kJ/mol^{-1}	$\Delta E_{D3BJ,}$ kJ/mol^{-1}	$\Delta E_{ads,}$ kJ/mol^{-1}	$\Delta E_{D3BJ,}$ kJ/mol^{-1}	$\Delta E_{ads,}$ kJ/mol^{-1}	$\Delta E_{D3BJ,}$ kJ/mol^{-1}	$\Delta E_{ads,}$ kJ/mol^{-1}	$\Delta E_{D3BJ,}$ kJ/mol^{-1}	
T6T6	-71	-17	-171	-41	-235	-69	-40	-29	1.12
T6T8	-80	-17	-181	-41	-242	-69	-47	-28	1.12
T8T8	-87	-18	-188	-41	-247	-69	-53	-28	1.12
T3T6	-90	-16	-198	-45	-254	-60	-54	-26	1.05
T3T8	-82	-17	-190	-44	-241	-62	-49	-27	1.04
T7T8	-82	-18	-187	-45	-243	-60	-51	-28	1.05
T2T6	-91	-15	-194	-41	-246	-68	-54	-25	1.05
T6T2	-92	-14	-200	-40	-243	-64	-53	-23	1.04
T4T7	-96	-14	-192	-40	-245	-62	-58	-24	1.06
T2T3	-120	-17	-236	-44	-280	-65	-77	-26	1.08
T3T2	-121	-19	-223	-38	-284	-71	-80	-31	1.03

Table S5. Selected geometrical parameters of the basic probes.

	CO		CH_3CN		C_5H_5N	CH_4
	d(Zn–C), Å	d(O–C), Å	d(Zn–N), Å	d(C–N), Å	d(Zn–N), Å	d(Zn–C), Å
T6T6	2.132	1.134	1.993	1.160	2.000	2.500
T6T8	2.115	1.133	1.970	1.158	1.983	2.440
T8T8	2.112	1.133	1.962	1.159	1.981	2.396
T3T6	2.075	1.133	1.945	1.159	1.989	2.336
T3T8	2.088	1.134	1.947	1.159	1.974	2.399
T7T8	2.097	1.134	1.953	1.158	1.981	2.416
T2T6	2.091	1.134	1.944	1.158	1.965	2.388
T6T2	2.069	1.133	1.932	1.159	1.953	2.351
T4T7	2.083	1.133	1.933	1.158	1.946	2.334
T2T3	2.044	1.133	1.912	1.159	1.929	2.312
T3T2	2.018	1.133	1.944	1.160	1.943	2.227

Table S6. Scaled vibrational frequencies of the basic probes' adsorption complexes.

	CO	CH_3CN	C_5H_5N	CH_4
	$\nu_{C\equiv O}$, cm^{-1}	$\nu_{C\equiv N}$, cm^{-1}	ν_{19}, cm^{-1}	ν_1, cm^{-1}
T6T6	2229	2315	1498	2870
T6T8	2238	2328	1499	2851
T8T8	2234	2324	1499	2858
T3T6	2233	2326	1494	2847
T3T8	2227	2326	1496	2853
T7T8	2224	2327	1494	2835
T2T6	2226	2330	1498	2824
T6T2	2235	2326	1499	2802
T4T7	2233	2332	1497	2798
T2T3	2239	2315	1497	2815
T3T2	2240	2325	1496	2735

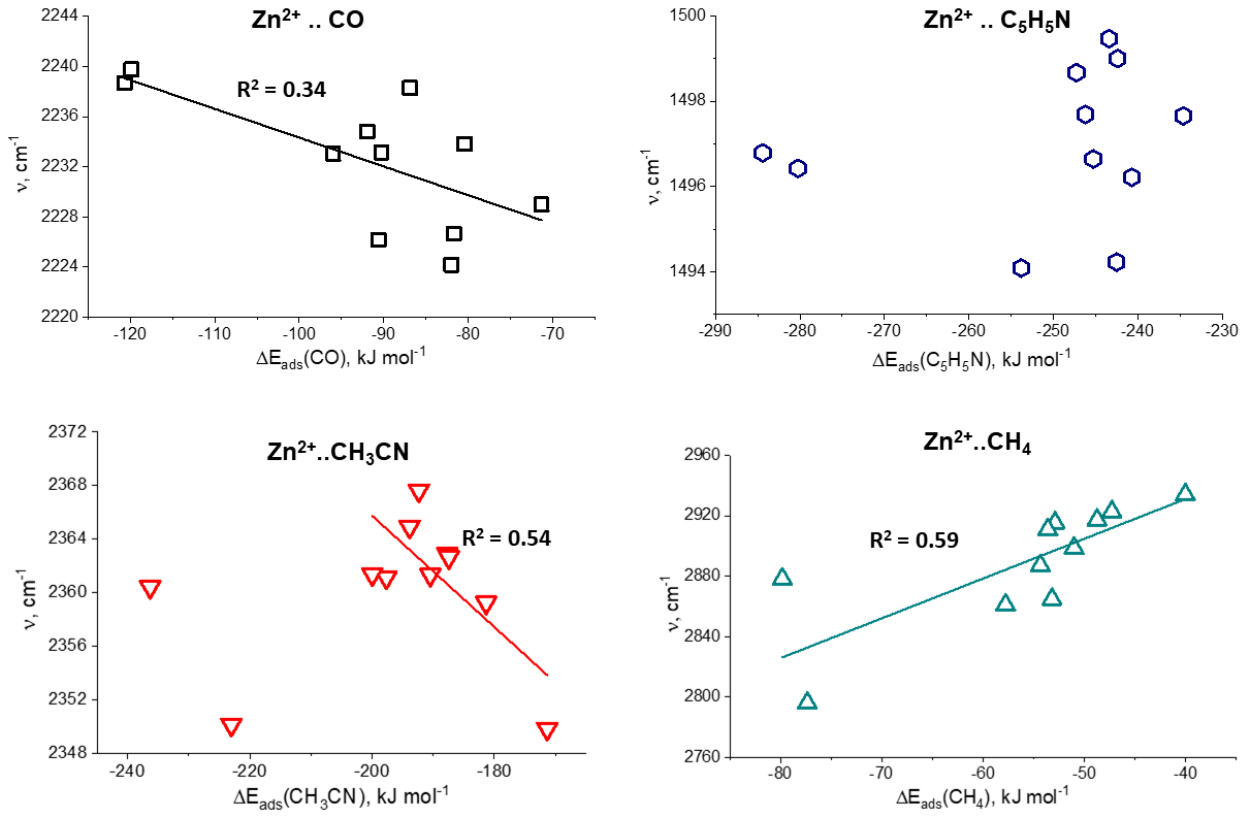

Figure S7. The relationships between adsorption energies of basic probes and respective vibrational frequencies.

Following vibrational modes, observed with FTIR technique, are considered: $\nu_{C\equiv O}$ stretching vibration for CO, $\nu_{C\equiv N}$ stretching vibration for CH_3CN, ν_{19a} mode for pyridine, and ν_1 symmetric C-H stretching vibration for methane. We established the relations between the adsorption energies and respective vibrational frequencies. The related plots are shown in Figure S7. The calculated IR frequencies are listed in Table S6. We found that respective frequencies of CO and C_5H_5N do not correlate with adsorption energies indicating that these frequencies do not reflect the Zn^{2+} adsorption energies. Interesting results obtained for relations between the adsorption energies of CH_3CN and the $\nu_{C\equiv N}$ stretching vibrations: there is linear correlation with $R^2 = 0.54$ for relatively stable sites, with complete breaking of these relations for unstable (T2T3 and T3T2) sites. Finally, we observe the linear correlations with $R^2 = 0.59$ for relations between the CH_4 adsorption energies and its ν_1 symmetric C-H stretching vibrations.

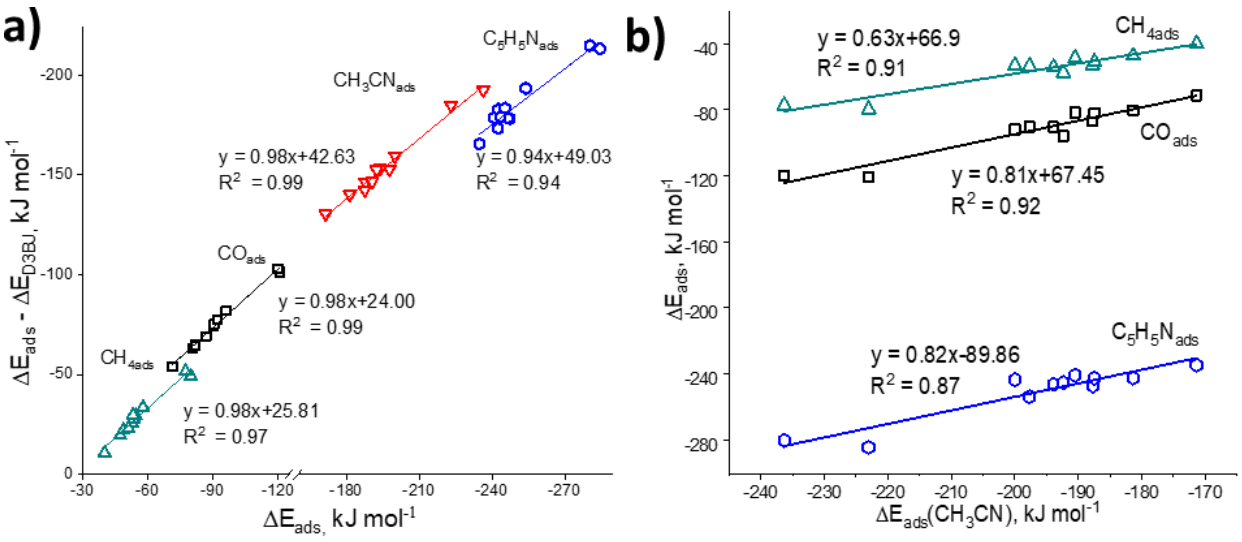

Figure S8. Demonstration of the dispersion effects on the probe adsorption energies for various locations in Zn-BEA zeolite (a). Computed adsorption energies of different basic probes in Zn-BEA zeolite as function of $\Delta E_{ads}(CH_3CN)$ (b).

The adsorption energies of these probes are affected not only by the basic strength of the probes and acidity of the Zn^{2+}, but by the different molecular sizes and various local geometry surrounding the active sites.[3] We illustrated the effects of dispersion interactions by the

demonstration of the correlation between the dispersion-corrected (ΔE_{ads}) and -uncorrected ($\Delta E_{ads} - \Delta E_{D3BJ}$) adsorption energy (Figure S8a). Dispersion interactions with the zeolite framework in case of small base molecules are insignificant, resulting in the- correlations with $R^2 = 0.99$. However, in the case of pyridine adsorption complexes the dispersion effects are slightly disturbing the correlation, lowering the R^2 coefficient to 0.94. Moreover, many points on pyridine graphic are concentrating in one area thus indicating that the local confinement around Zn^{2+} could affect pyridine adsorption energy significantly, potentially make pyridine less accurate probe to measure Zn^{2+} Lewis acidity. While interaction of the small base molecules with zeolite lattice is insignificant, the local confinement around Zn^{2+} could affect pyridine adsorption energy significantly, potentially make pyridine less accurate probe to measure Zn^{2+} Lewis acidity.

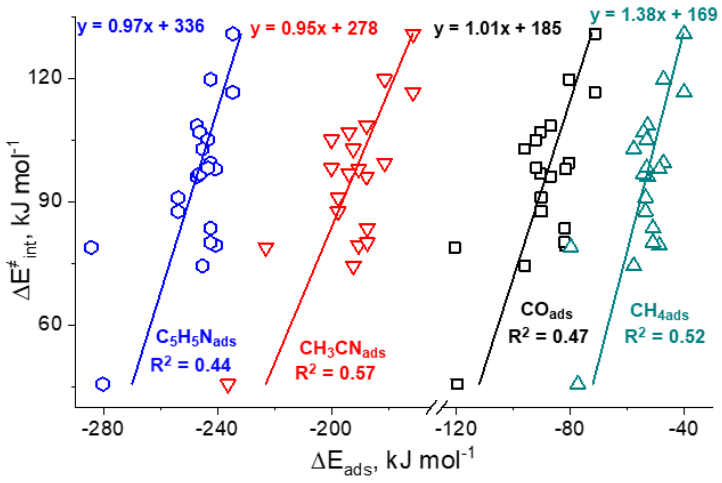

Figure S9. The relations between the activation barriers and ΔE_{ads} of basic probes.

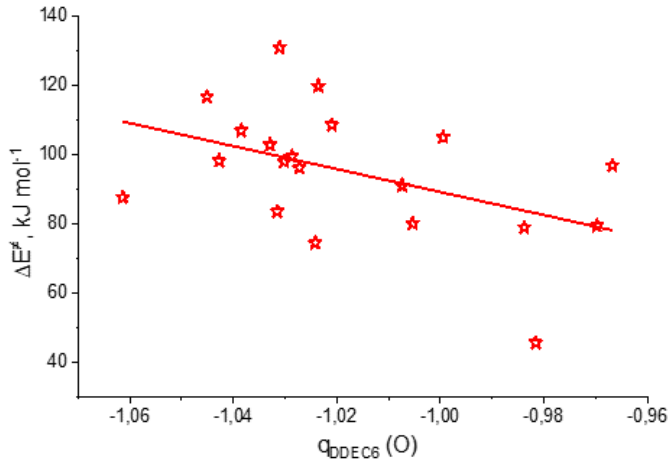

Figure S10. Relations between activation barriers and DDEC6 charges of O atoms (a) or hydrogen affinity (b).

Table S7. E_H and q_{DDEC6} (O) values.

Configuration	E_H, kJ/mol	q_{DDEC6} (O)	Configuration	E_H	q_{DDEC6} (O)
T6T6O1	277	-1.03	T7T8O1	165	-1.01
T6T6O2	302	-1.05	T7T8O2	150	-1.03
T6T8O1	205	-1.03	T2T6O1	168	-1.04
T6T8O2	199	-1.02	T2T6O2	195	-0.97
T8T8O1	191	-1.03	T6T2O1	187	-1.00
T8T8O2	193	-1.02	T6T2O2	166	-1.04
T3T6O1	191	-1.06	T4T7O1	163	-1.02
T3T6O2	178	-1.01	T4T7O2	145	-1.03
T3T8O1	172	-1.03	T2T3O1	114	-0.98
T3T8O2	180	-0.97	T3T2O1	116	-0.98

Table S8. Adsorption energies and selected geometrical of pyrrole and methylacetylene adsorption complexes. The N–H bond orders of the pyrrole are also listed. The O_z denotes zeolite oxygen atom.

	Pyrrole					Methylacetylene			
	$\Delta E_{ads,}$ kJ/mol^{-1}	ΔE_{D3BJ}, kJ/mol^{-1}	d(N–H), Å	d(H–O_z), Å	Bond order (N–H)	$\Delta E_{ads,}$ kJ/mol^{-1}	ΔE_{D3BJ}, kJ/mol^{-1}	d(C–H), Å	d(H–O_z), Å
T6T6O1	-103	-64	1.029	2.352	0.746	-68	-37	1.081	2.505
T6T6O2	-116	-60	1.030	2.370	0.741	-114	-39	1.082	2.608
T6T8O1	-154	-57	1.060	1.780	0.691	-129	-39	1.119	1.838
T6T8O2	-101	-62	1.037	2.351	0.728	-125	-39	1.087	2.543
T8T8O1	-148	-57	1.053	1.828	0.709	-158	-42	1.104	1.875
T8T8O2	-132	-64	1.039	2.128	0.728	*	*	*	*
T3T6O1	-156	-62	1.044	1.892	0.718	-162	-47	1.091	1.998
T3T6O2	-145	-66	1.037	2.108	0.720	-137	-44	1.089	2.218
T3T8O1	-146	-64	1.038	2.226	0.735	-147	-41	1.085	2.297
T3T8O2	-152	-63	1.041	2.024	0.712	-118	-36	1.111	1.885
T7T8O1	-137	-69	1.044	1.951	0.709	-111	-41	1.097	2.029
T7T8O2	-137	-62	1.034	2.307	0.730	-136	-48	1.081	2.476
T2T6O1	-130	-62	1.046	1.908	0.705	-123	-38	1.089	2.250
T2T6O2	-122	-55	1.042	1.919	0.702	-98	-37	1.112	1.959
T6T2O1	-130	-58	1.032	2.187	0.729	-122	-36	1.086	2.188
T6T2O2	-142	-61	1.038	2.123	0.720	-141	-37	1.085	2.593
T4T7O1	-168	-56	1.057	1.770	0.700	-167	-34	1.104	1.867
T4T7O2	-118	-61	1.036	2.184	0.722	-122	-35	1.084	2.450
T2T3O1	-205	-63	1.039	2.286	0.666	-197	-37	1.113	1.791
T3T2O1	-153	-67	1.071	1.671	0.720	-148	-39	1.097	2.241

*The adsorption complex of propyne on T8T8O2 structure cannot not be stabilized due to the proximity of O1 atom that has higher basicity than O2 atom, and the complex geometry optimization always results propyne adsorption on O1 atom.

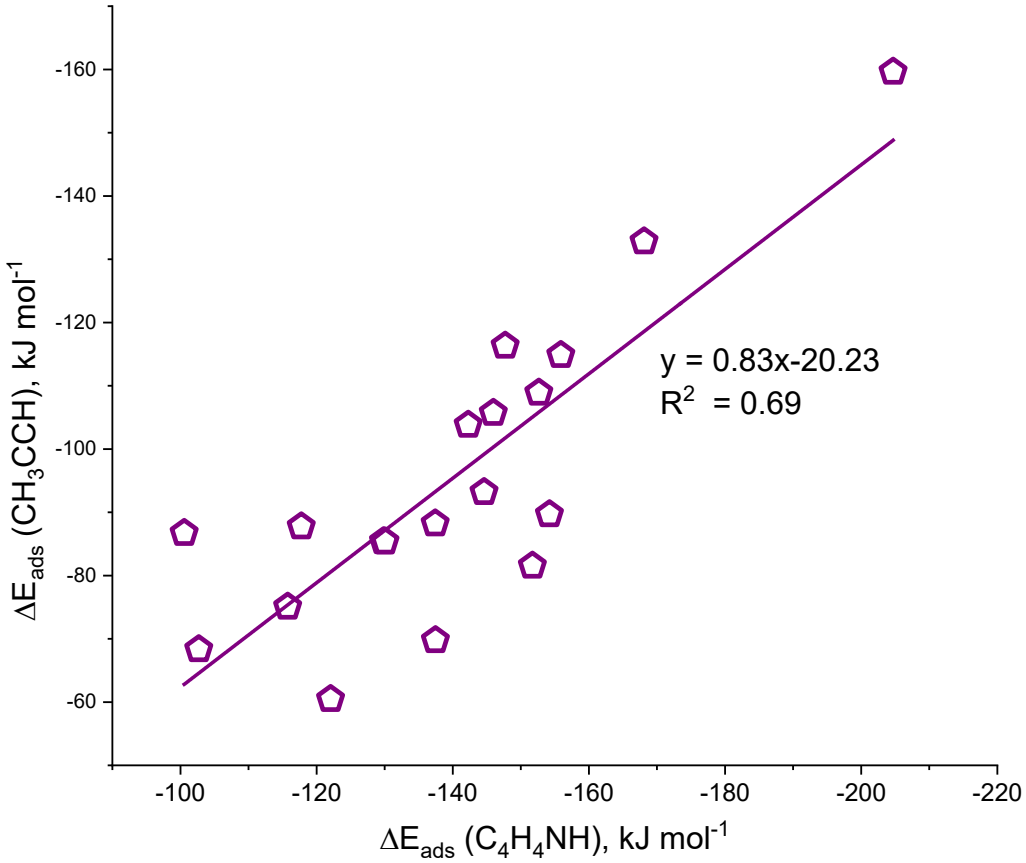

Figure S11. Relations of the adsorption energies of pyrrole and propyne.

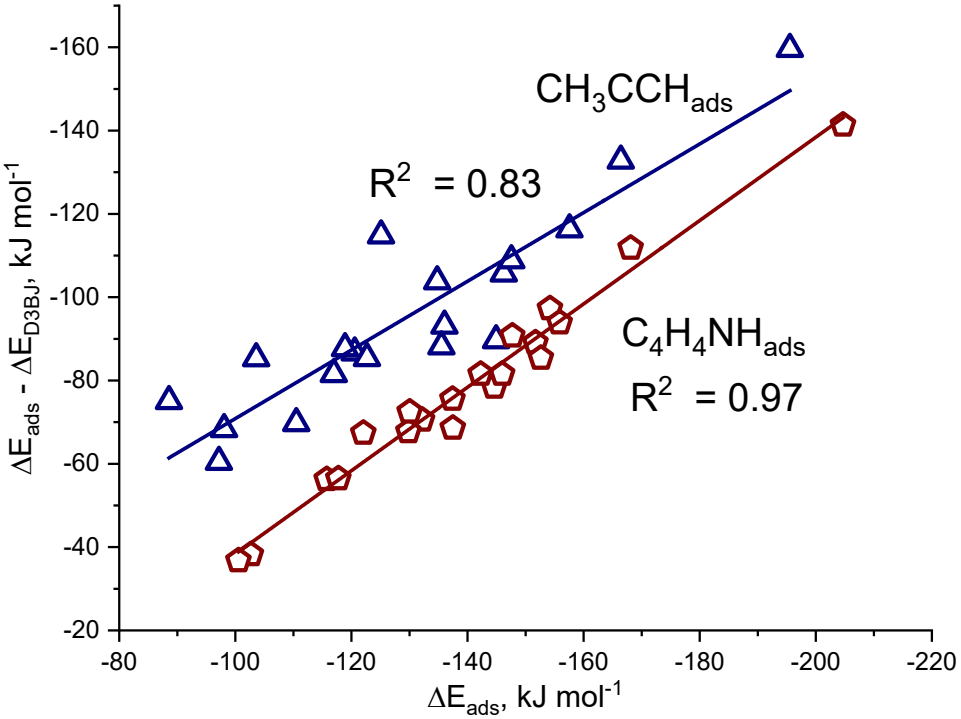

Figure S12. Demonstration of the dispersion effects on the pyrrole and propyne adsorption energies for various locations in Zn-BEA zeolite

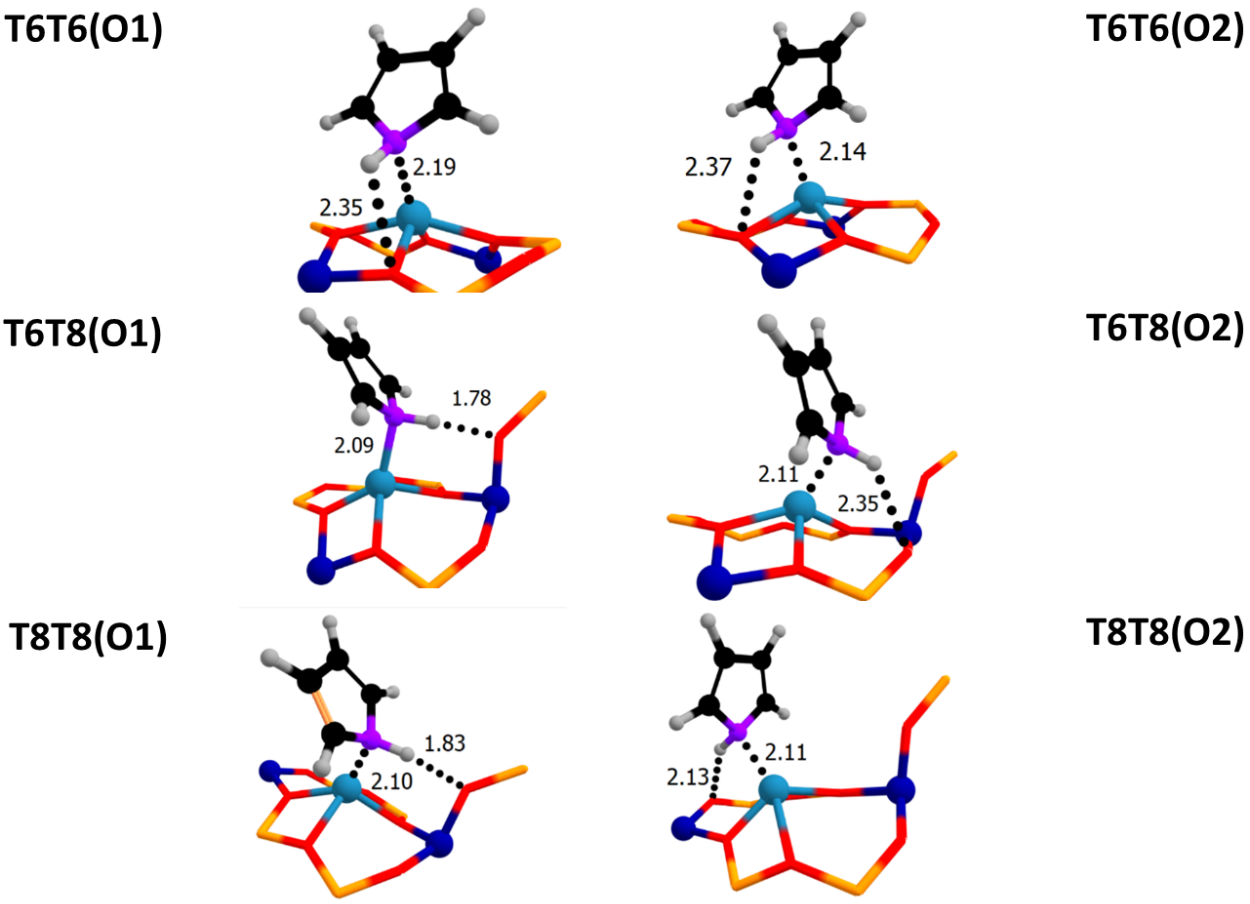

Figure S13. Geometries of the pyrrole adsorption complexes of T6T6, T6T8 and T8T8 configurations.

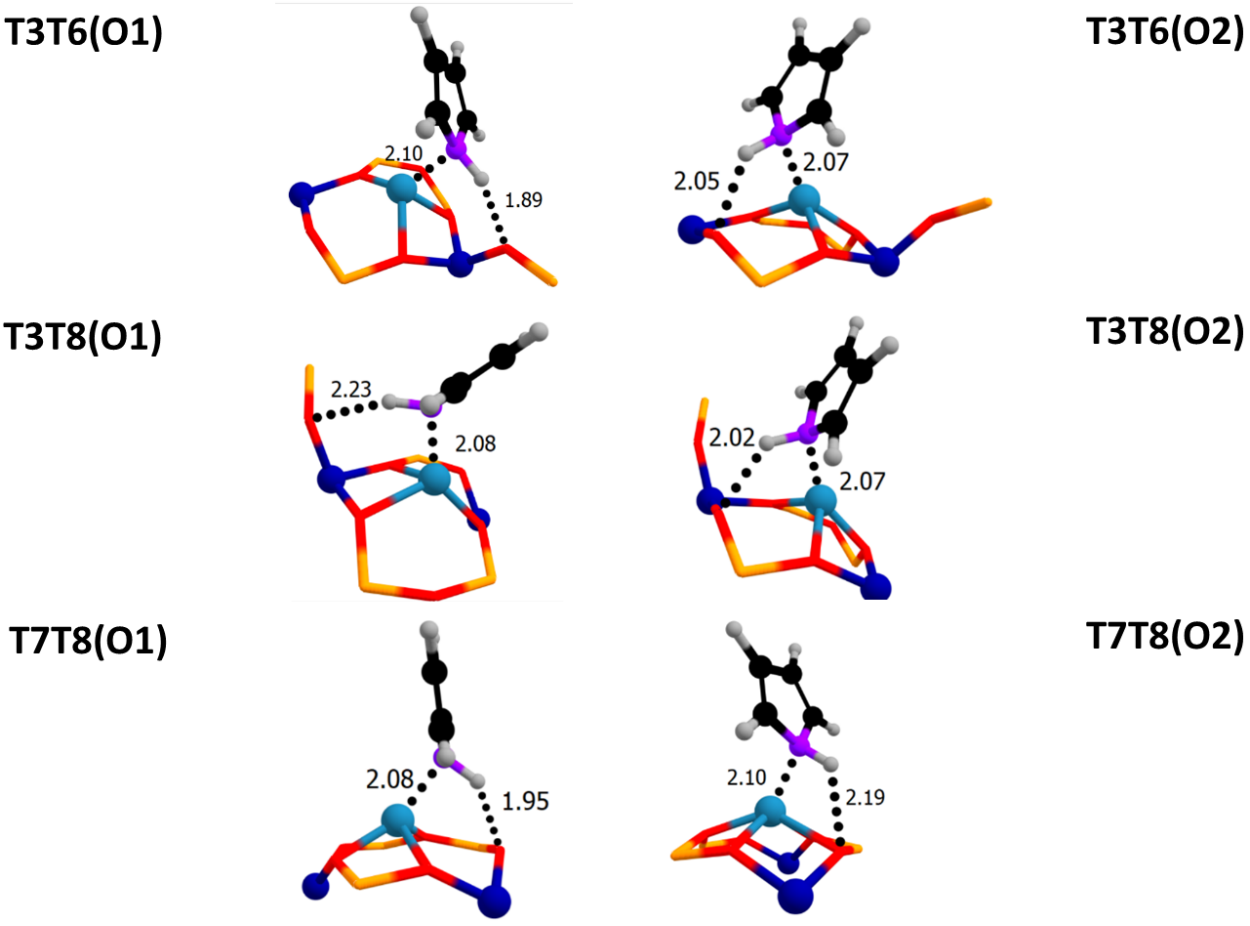

Figure S14. Geometries of the pyrrole adsorption complexes of T3T6, T3T8 and T7T8 configurations.

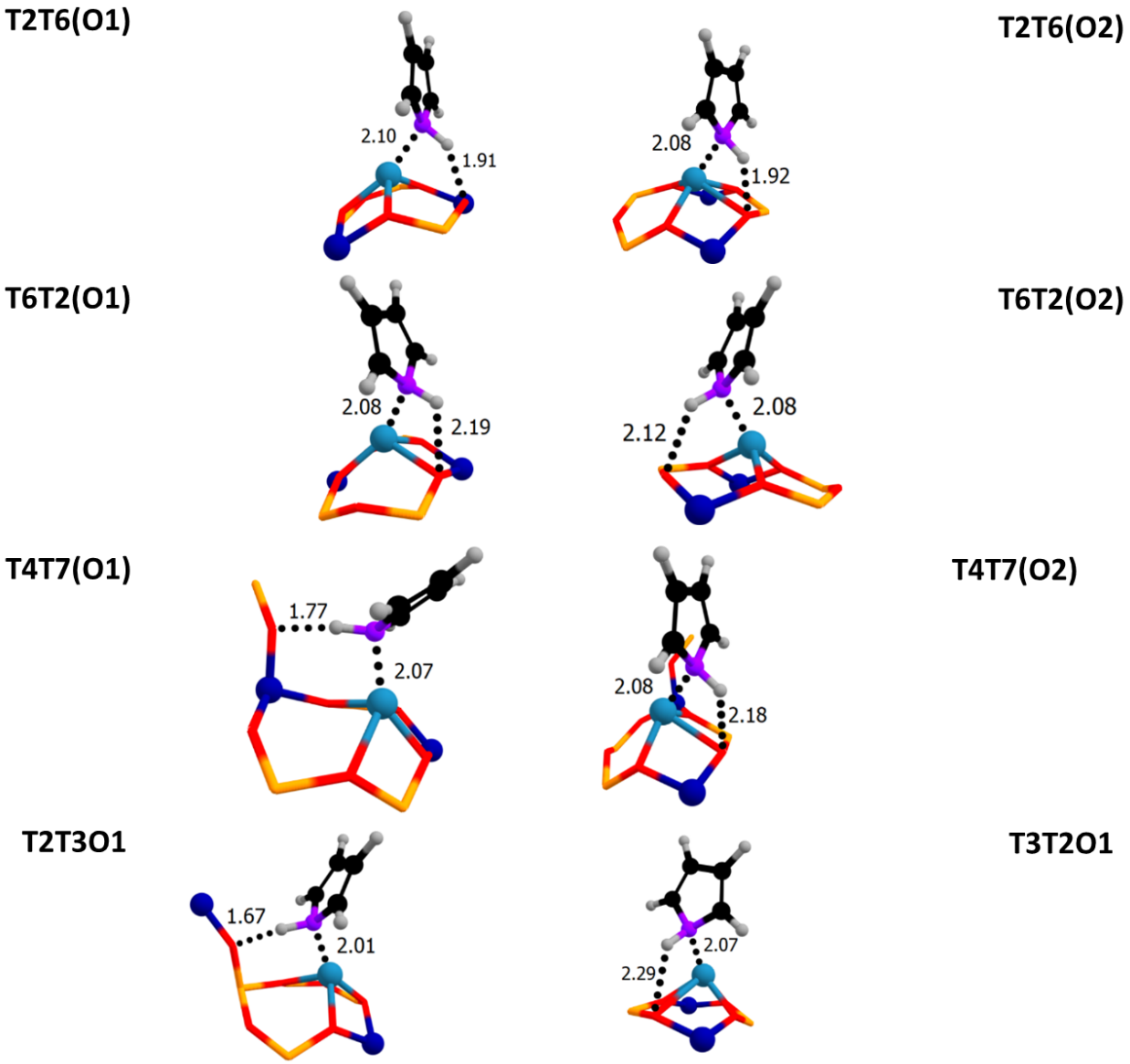

Figure S15. Geometries of the pyrrole adsorption complexes of T2T6, T6T2, T4T7, T2T3 and T3T2 configurations.

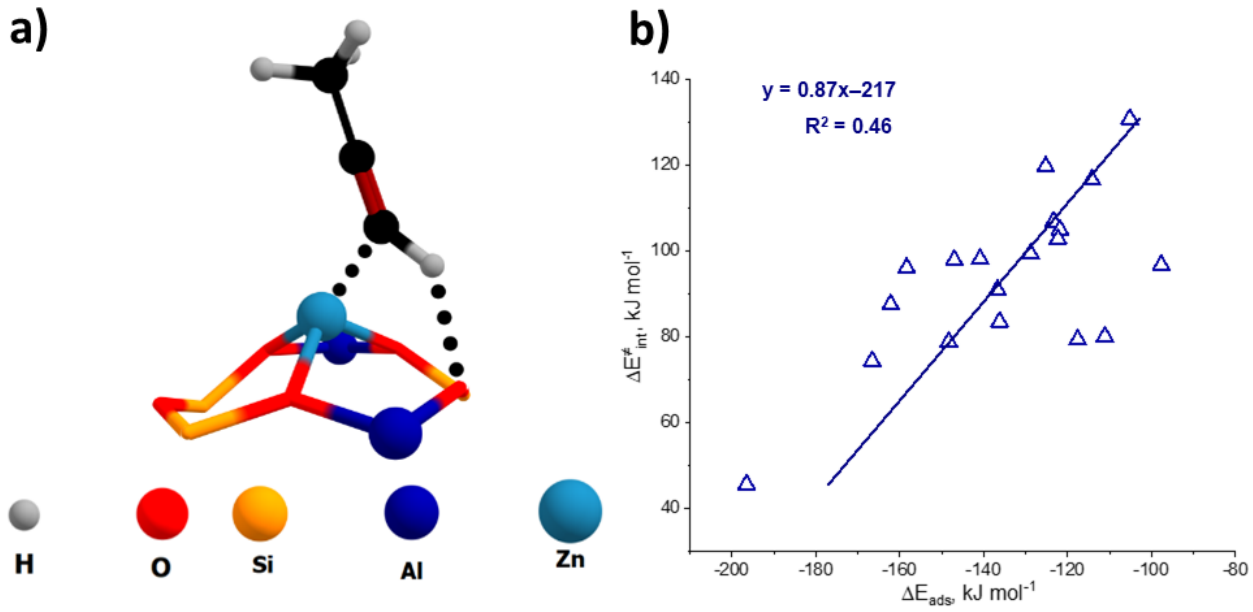

Figure S16. Geometry of the propyne adsorption complex (a). Correlations between intrinsic activation barrier and propyne adsorption energies (b).

Table S9. Scaled N–H and C–H vibrational frequencies for pyrrole and methylacetylene respectively.

Configuration	ν(N–H)	ν(C–H)	Configuration	ν(N–H)	ν(C–H)
T6T6O1	3278	3186	T7T8O1	3040	2774
T6T6O2	3273	3174	T7T8O2	3228	2971
T6T8O1	2783	2673	T2T6O1	3006	3191
T6T8O2	3179	3111	T2T6O2	3073	3087
T8T8O1	2889	2862	T6T2O1	3238	2788
T8T8O2	3128	*	T6T2O2	3144	3137
T3T6O1	3017	3027	T4T7O1	2811	3139
T3T6O2	3122	3083	T4T7O2	3193	2862
T3T8O1	3146	3138	T2T3O1	2610	2983
T3T8O2	3101	3186	T3T2O1	3160	3154

*The adsorption complex of propyne on T8T8O2 structure cannot not be stabilized due to the proximity of O1 atom that has higher basicity than O2 atom, and the complex geometry optimization always results propyne adsorption on O1 atom.

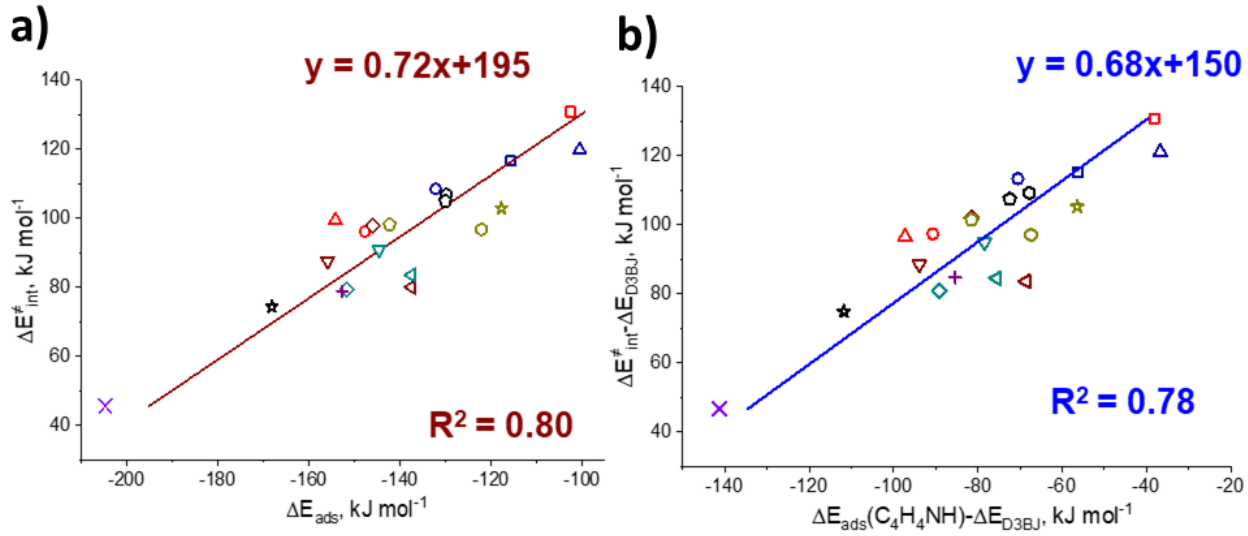

Figure S17. Correlations between intrinsic activation barrier and pyrrole adsorption energies for Zn-BEA with (a) and without (b) dispersion interactions.

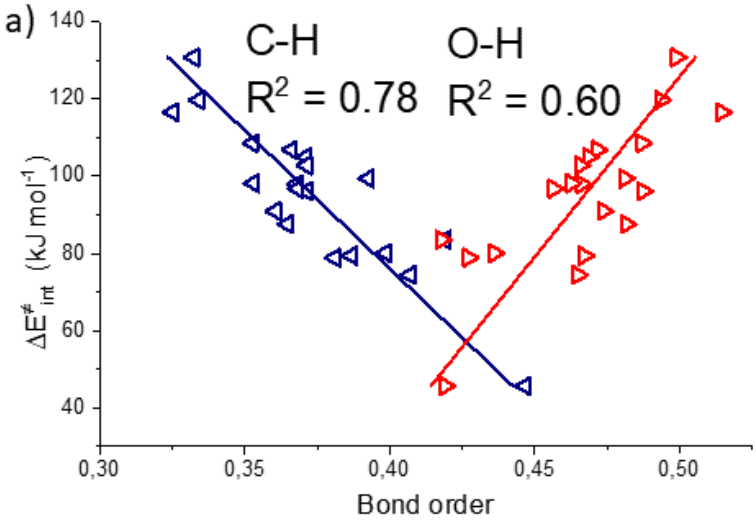

Figure S18. Relations between the activation barriers and bond orders of the O–H and C–H bonds in the methane activation transition state geometries.

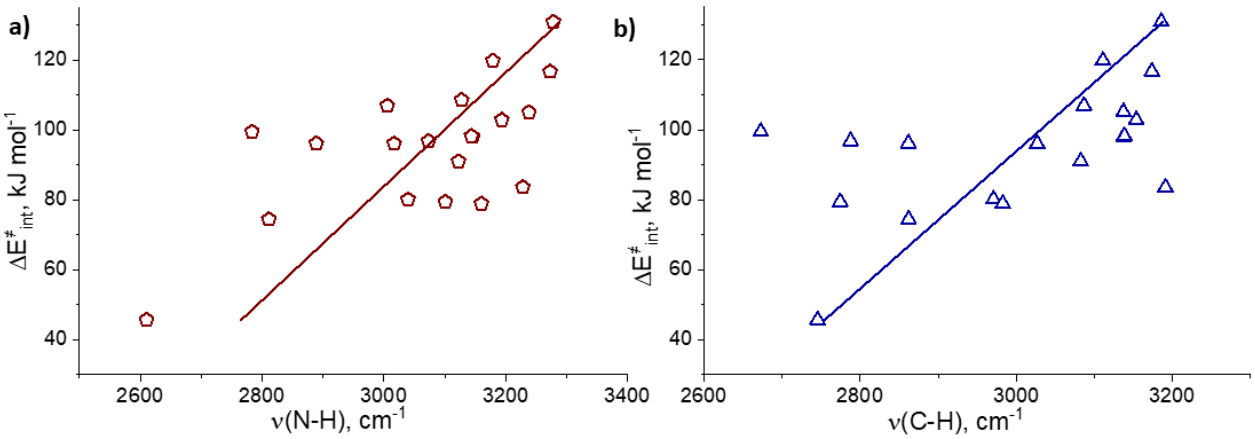

Figure S19. Relations between activation barriers and N–H (a) or C–H (b) frequencies of pyrrole and propyne adsorption complexes. All values are listed in Table S16

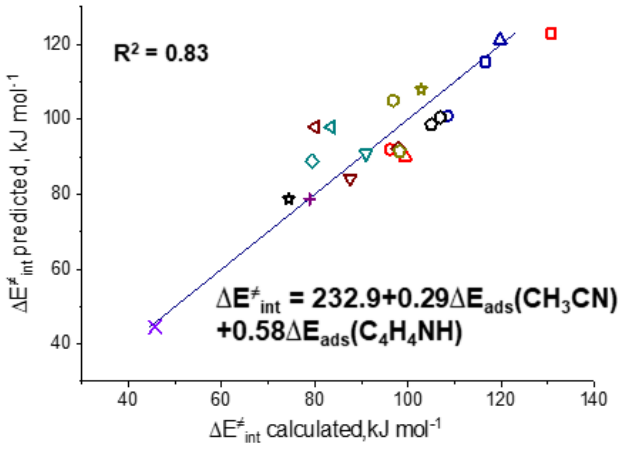

Figure S20. Two-dimensional correlations between the $\Delta E_{int}^{\neq}$ and the linear combination of ΔE_{ads} (CH_3CN) and ΔE_{ads} (C_4H_4NH).

Table S10. *p*-values for the coefficients in the respective linear relations. The coefficient is statistically significant if $p<0.05$.

Correlation	p-values
$\Delta E^{\neq}_{int} = 232.9+0.29\Delta E_{ads}(CH_3CN)+0.58\Delta E_{ads}(C_4H_4NH)$	10^{-5} (E_{ads} (C_4H_4NH); 0.06(E_{ads}(CH_3CN))
$\Delta E^{\neq}_{int} = 149.6+0.13E_H+0.57\Delta E_{ads}(C_4H_4NH)$	10^{-5}(C_4H_4NH); 10^{-3}(E_H)

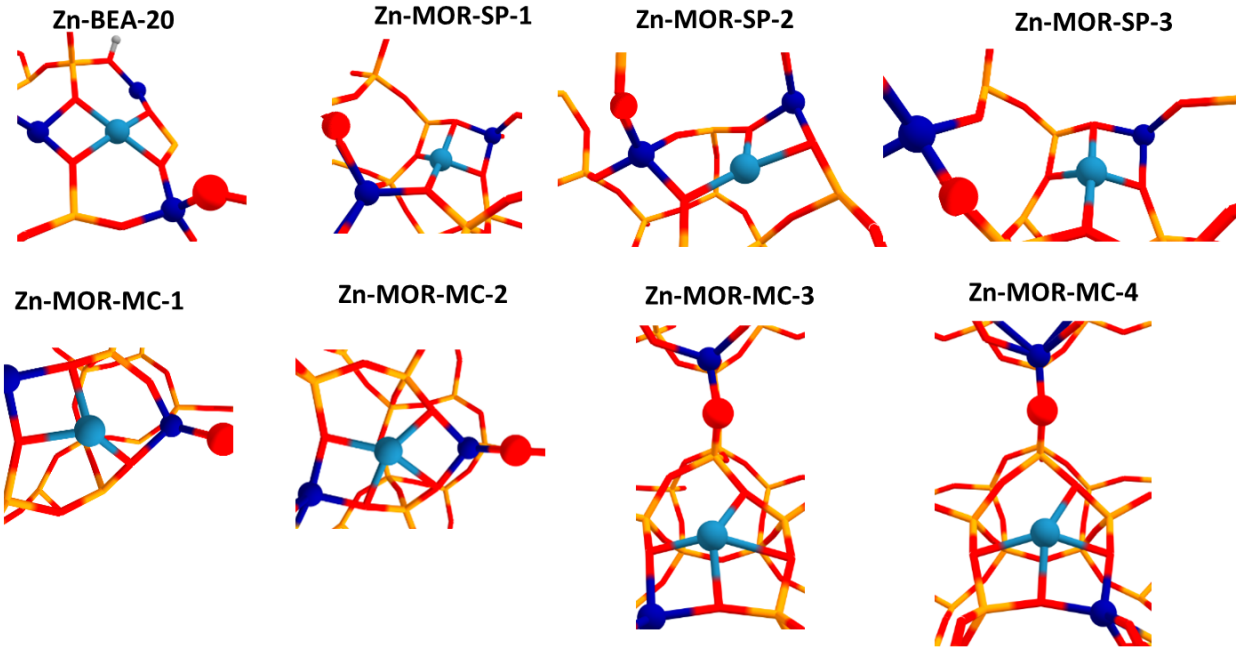

Figure S21. The structures of the additional zeolite models.

Table S11. DFT-calculated and predicted using the obtained correlation activation barriers for methane activation. All values are given in kJ mol^{-1}.

	DFT-Calculated $\Delta E_{int}^{\neq}$	$\Delta E_{int}^{\neq}(\Delta E_{ads}[C_4H_4NH])$	$\Delta E_{int}^{\neq}$ ($\Delta E_{ads}[C_4H_4NH]$, $\Delta E_{ads}[CH_3CN]$)	$\Delta E_{int}^{\neq}$ (ΔE_{ads} [C_4H_4NH], E_H)
Zn-BEA-20	93	86	93	90
Zn-MOR	82	101	117	99

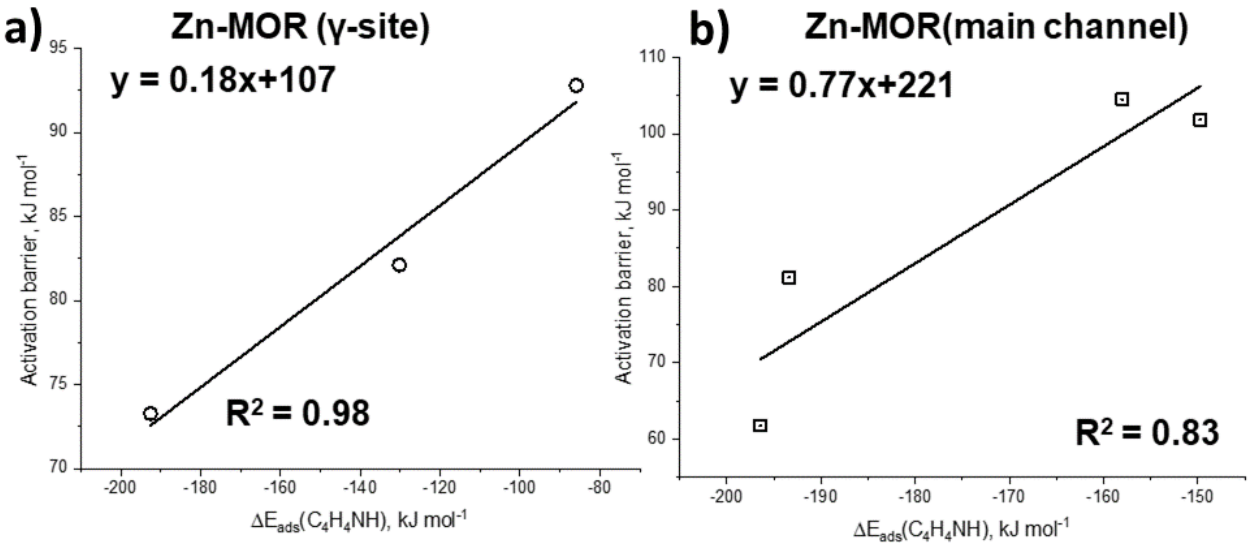

Figure S22. Correlations between intrinsic activation barrier and pyrrole adsorption energies for different Zn sites in the γ-site of Zn-MOR "side pocket" (a) and in the main channel of Zn-MOR (b).

Table S12. The number of short (D < 2.5 Å) and long (D < 3.0 Å, in parenthesis) CH···O contacts in the considered pyrrole adsorption complexes.

System	n(CH···O)	System	n(CH···O)
T6T6O1	1 (8)	T7T8O1	0 (7)
T6T6O2	0 (1)	T7T8O2	0 (2)
T6T8O1	0 (2)	T2T6O1	0 (3)
T6T8O2	0 (3)	T2T6O2	0 (4)
T8T8O1	0 (2)	T6T2O1	0 (3)
T8T8O2	0 (3)	T6T2O2	0 (1)
T3T6O1	0 (3)	T4T7O1	0 (3)
T3T6O2	0 (6)	T4T7O2	0 (4)
T3T8O1	0 (2)	T2T3O1	1 (2)
T3T8O2	0 (6)	T3T2O1	2 (6)
BEA-3Al	0 (0)	Zn-MOR-SP1	4 (13)
Zn-MOR-SP2	5(13)	Zn-MOR-SP3	3(14)
Zn-MOR-MC1	1(3)	Zn-MOR-MC2	0(0)
Zn-MOR-MC3	0(0)	Zn-MOR-MC4	0(0)

References

(1) Zhidomirov, G. M.; Shubin, A. A.; Kazansky, V. B.; Van Santen, R. A., Possible Molecular Structure of Promoted Lewis Acidity Sites in ZnZSM-5. *Int. J. Quantum Chem.* **2004**, *100*, 489–494.
(2) Pidko, E. A.; van Santen, R. A., Activation of Light Alkanes Over Zinc Species Stabilized in ZSM-5 Zeolite: A Comprehensive DFT Study. *J. Phys. Chem. C* **2007**, *111*, 2643–2655.
(3) Liu, C.; Tranca, I.; van Santen, R. A.; Hensen, E. J. M.; Pidko, E. A., Scaling Relations for Acidity and Reactivity of Zeolites. *J. Phys. Chem. C* **2017**, *121*, 23520-23530.